ACS Catalysis

Research Article

pubs.acs.org/acscatalysis

Fe-Based MOFs for Photocatalytic CO_2 Reduction: Role of Coordination Unsaturated Sites and Dual Excitation Pathways

Dengke Wang,[†] Renkun Huang,[†] Wenjun Liu, Dengrong Sun, and Zhaohui Li*

Research Institute of Photocatalysis, State Key Laboratory of Photocatalysis on Energy and Environment, College of Chemistry, Fuzhou University, Fuzhou 350002, People's Republic of China

Supporting Information

ABSTRACT: The utilization of solar energy for the conversion of CO_2 into valuable organic products is one of the best solutions to solve the problems of global warming and energy shortage. The development of photocatalysts capable of reducing CO_2 under visible light, especially those containing earth-abundant metals, is significant. Herein we report that a series of earth-abundant Fe-containing MOFs (MIL-101(Fe), MIL-53(Fe), MIL-88B(Fe)) show photocatalytic activity for CO_2 reduction to give formate under visible light irradiation. The direct excitation of the Fe−O clusters in these MOFs induces the electron transfer from O^{2-} to Fe^{3+} to form Fe^{2+}, which is responsible for the photocatalytic CO_2 reduction. Among the three investigated Fe-based MOFs, MIL-101(Fe) showed the best activity due to the existence of the coordination unsaturated Fe sites in its structure. All three amine-functionalized Fe-containing MOFs (NH_2-MIL-101(Fe), NH_2-MIL-53(Fe) and NH_2-MIL-88B(Fe)) showed enhanced photocatalytic activity in comparison to the unfunctionalized MOF, due to the existence of dual excitation pathways: i.e., excitation of an NH_2 functionality followed by an electron transfer to the Fe center in addition to the direct excitation of Fe−O clusters.

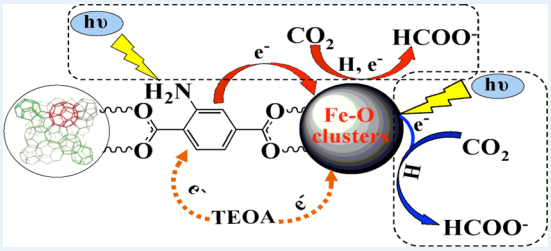

KEYWORDS: *photocatalytic CO_2 reduction, visible light, metal−organic frameworks, coordination unsaturated sites, dual excitation pathway*

INTRODUCTION

The utilization of solar energy for the conversion of CO_2 into valuable organic products is one of the best solutions to solve the problems of global warming and energy shortage.[1] To date, various photocatalysts, including inorganic semiconductors, metal-incorporated zeolites, and homogeneous transition-metal complexes, have been developed and their photocatalytic performance for CO_2 reduction has been investigated.[2] Most of the semiconductor photocatalysts investigated can use water as a reductant; however, they are only active in the UV region and their efficiency for CO_2 reduction is still quite low. On the other hand, homogeneous molecular systems show a relatively high efficiency for solar CO_2 fixation in the presence of strong organic sacrificial agents. Unfortunately, most of the involved molecular systems are limited to noble-metal catalysts. It is therefore of great significance to develop efficient photocatalysts composed of earth-abundant transition metals which are capable of reducing CO_2 under visible light.

Metal−organic frameworks (MOFs), constructed from metal clusters interconnected by multidentate organic linkers, are a class of three-dimensional crystalline porous hybrid materials. Their inherent large surface areas, uniform but tunable cavities, and tailorable chemistry have enabled them to show a variety of potential applications.[3−9] Previous studies on MOF-5 have revealed that the organic linkers in MOF-5 can act as antennas to absorb light upon irradiation and activate the metal clusters, which is similar to the case for inorganic semiconductor quantum dots, via linker to metal cluster charge transfer (LCCT).[10] This and the structural analogy between MOFs and zeolites make MOFs promising photocatalysts. Actually, several studies that demonstrate the successful applications of MOFs in photocatalysis, mostly for photocatalytic dye degradation or hydrogen production, have emerged.[11,12] As photocatalysts, MOFs are superior to semiconductors, since their light absorption ability can be more easily tuned by modifications on the metal ions and the organic linkers to achieve an efficient utilization of solar energy. For example, Lin et al. reported that Uio-67(Zr) doped with an Re(I) complex shows photocatalytic activity for CO_2 reduction.[11f] Recently, by facile ligand substitutions, our group successfully obtained NH_2-MIL-125(Ti) and NH_2-Uio-66(Zr), which are active in photocatalytic CO_2 reduction under visible light irradiation.[12] These studies demonstrate the high potential of using MOFs as photocatalysts. However, studies on MOF-based photocatalysis are still in the infancy stage, considering the large number of MOF materials that have already been reported.

Although a previous study on NH_2-MIL-125(Ti) indicates that Ti^{3+} is involved in photocatalytic CO_2 reduction, a great deal remains unclear about this photocatalytic process. It is therefore indispensable to explore the performance for CO_2

Received: August 11, 2014
Revised: October 18, 2014
Published: October 21, 2014

reduction over that of other MOFs with redox-active metal centers and elucidate factors influencing photocatalytic performance. Fe-based MOF materials are extremely attractive, since iron is an earth-abundant element and iron-containing complexes are commonly used in catalysis and photocatalysis.[13] Moreover, another advantage of using Fe-based MOF materials for photocatalysis is that almost all of the Fe-based MOF materials already reported are visible-light-responsive due to the existence of extensive iron oxo clusters, which makes it possible for a direct excitation of the Fe−O clusters upon visible light irradiation.[11g,14]

Herein we report the photocatalytic performance for CO_2 reduction over three typical Fe-based MOFs (MIL-101(Fe), MIL-53(Fe), and MIL-88B(Fe)) and their amino-functionalized derivatives. These Fe-based MOF materials have been chosen since they all contain a similar organic linker, BDC (BDC = benzene-1,4-dicarboxylate), but have quite different structures. All three chosen Fe-based MOFs themselves are responsive to visible light. The photocatalytic results show that all of these Fe-based MOFs can reduce CO_2 under visible light irradiation and that direct excitation on the Fe−O clusters to induce electron transfer from O^{2-} to Fe^{3+} is responsible for the photocatalytic CO_2 reduction. A comparison of the performance among the three Fe-based MOFs indicates that the photocatalytic performance is significantly influenced by the structure of the MOF. Their amino-functionalized derivatives (NH_2-MIL-101(Fe), NH_2-MIL-53(Fe), and NH_2-MIL-88B-(Fe)) show enhanced photocatalytic performance for CO_2 reduction as compared to the unfunctionalized MOFs. For the first time, a dual-excitation pathway for their enhanced performance has been elucidated.

RESULTS AND DISCUSSION

MIL-101(Fe) was prepared from $FeCl_3$ and H_2BDC following the reported method.[15] It has a rigid zeotype crystal structure, consisting of quasi-spherical cages of two modes (2.9 and 3.4 nm) accessible through windows of ca. 1.2 and 1.6 nm, respectively. The XRD pattern of the as-prepared product as shown in Figure 1 confirms the formation of a pure phase of

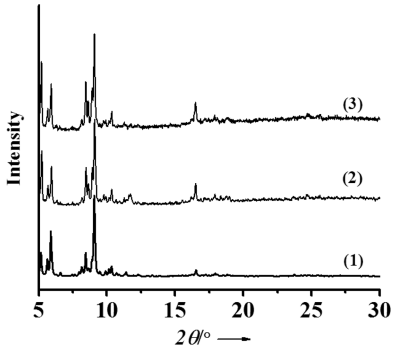

Figure 1. XRD patterns: (1) calculated sample; (2) MIL-101(Fe); (3) NH_2-MIL-101(Fe).

MIL-101(Fe). TG and N_2 adsorption/desorption studies indicate that MIL-101(Fe) with high quality has been successfully obtained (Figures S1 and S2, Supporting Information). The UV−vis DRS spectrum of the as-prepared MIL-101(Fe) shows a broad intense absorption in 200−450 nm region, which can be further deconvoluted into one absorption band located at ca. 270 nm and one band extending into the visible region (Figure 2). The band at ca. 270 nm is attributed to the oxygen to iron charge transfer of isolated iron

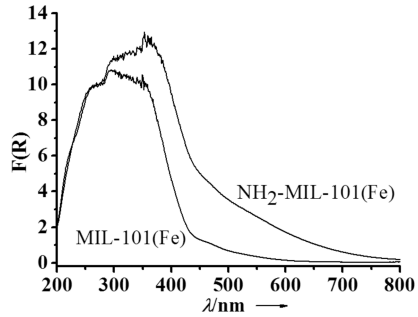

Figure 2. UV-DRS spectra of MIL-101(Fe) and NH_2-MIL-101(Fe).

in an octahedral coordination environment, while the other band extending into the visible light region can be ascribed to the existence of Fe_3O clusters in MIL-101(Fe). Previous studies have revealed that the existence of extensive iron clusters in the structure can lead to a red shift of the oxygen to iron charge transfer, even to the visible light region.[14]

The photocatalytic reduction of CO_2 over MIL-101(Fe) was performed under visible light irradiation. In the presence of TEOA as the sacrificial agent, the amount of $HCOO^-$ produced in 8 h is 59 μmol, which is much higher than that observed previously over NH_2-MIL-125(Ti) (Figure 3).[12a] No other

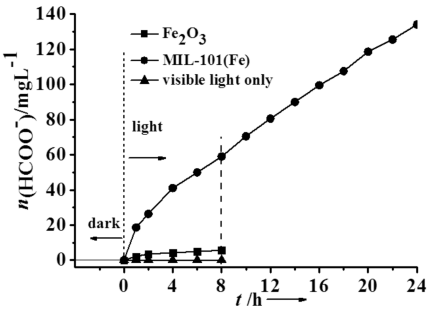

Figure 3. Amount of $HCOO^-$ produced as a function of the irradiation time over MIL-101(Fe), with Fe_2O_3 and visible light only. Conditions: photocatalyst 50 mg, MeCN/TEOA (5/1), solution volume 60 mL.

products have been detected in both the gas phase and liquid phase, suggesting that this reaction over MIL-101(Fe) has high selectivity. In contrast, no $HCOO^-$ was produced in the absence of MIL-101(Fe), TEOA, or visible light. Using Fe_2O_3 as the photocatalyst under otherwise similar reaction conditions gave only 5.6 μmol of $HCOO^-$. All of these observations indicate that MIL-101(Fe) can selectively photocatalytically reduce CO_2 to produce $HCOO^-$ under visible light irradiation. To study the origin of the $HCOO^-$, isotopic $^{13}CO_2$ has been used to carry out the photocatalytic reaction and the product obtained was identified by ^{13}C NMR. ^{13}C NMR spectra of the product obtained from the reaction with $^{12}CO_2$ shows only peaks corresponding to CD_3CN and TEOA (Figure S3, Supporting Information), while three additional peaks at 125.76, 159.64, and 165.42 ppm, which can be assigned to dissolved CO_2, HCO^{3-}, and $HCOO^-$, respectively, are observed over the product obtained from the reaction with $^{13}CO_2$ (Figure S4, Supporting Information). The isotopic $^{13}CO_2$ reaction confirms that the produced $HCOO^-$ actually

dx.doi.org/10.1021/cs501169t | ACS Catal. 2014, 4, 4254−4260

comes from CO_2. The TON observed for MIL-101(Fe) was determined to be ca. 1.2 in a 24 h reaction (Figure 3). Although this value is slightly lower in comparison to those for some already reported photocatalytic systems for CO_2 reduction, such as Re(I) complex doped Uio-67(Zr) (TON in 6 h: 5.0) and $[Ru(bpy)_2(CO)_2][PF_6]_2$/N−$Ta_2O_5$ hybrid system (saturated TON: ca. 5.0), the larger than 1.0 TON in the current system definitely suggests that the reaction is catalytic.[11f,k] To verify the nature of the catalyst, a filtrate reaction was carried out. It was found that the production of $HCOO^-$ ceased after the solid photocatalyst was removed from the reaction system at 8 h (Figure S5, Supporting Information). The filtrate reaction confirms that the reaction over MIL-101(Fe) is truly heterogeneous. The recycling use of the photocatalyst for three runs showed no obvious decrease of the photocatalytic activity (Figure S6, Supporting Information). In addition to this, the XRD, IR, TG, and N_2 adsorption of the photocatalyst after the reaction did not show many changes and the ICP of the filtrate reveals no leaching of the Fe^{3+} (Figures S7−S10, Supporting Information). All of these data suggest that MIL-101(Fe) is stable during the photocatalytic reaction.

To elucidate the semiconducting properties of MIL-101(Fe) upon light excitation, the Mott−Schottky method was applied to estimate its flat band position.[16] The flat band position for MIL-101(Fe) is determined to be −0.52 V vs NHE (Figure S11, Supporting Information). This value is more negative than the reduction potential of CO_2 to form formate (−0.28 V vs NHE), indicating that the iron oxo clusters in MIL-101(Fe) can reduce CO_2 to form formate. ESR studies were also carried out to detect the active species involved in the photocatalytic reaction. As shown in Figure 4, the original reaction system

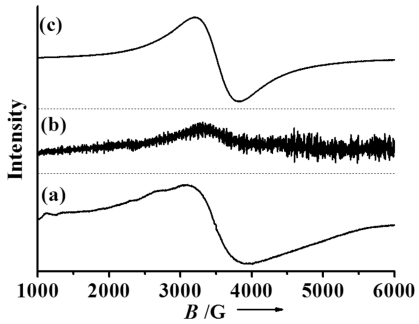

Figure 4. ESR spectra of a mixture of MIL-101(Fe) and TEOA: (a) in the dark; (b) upon irradiation; (c) in the presence of CO_2 upon irradiation.

(including MIL-101(Fe) and TEOA) in the dark gives a typical ESR signal ascribed to Fe^{3+} in octahedral FeO_6.[17] When visible light is irradiated on the above reaction system, the above ESR signal is quenched. This phenomenon can be well explained by a charge transfer from O^{2-} to Fe^{3+} and the formation of Fe^{2+} in MIL-101(Fe) upon visible light irradiation. The further addition of CO_2 into the above system can recover the ESR signal of Fe^{3+}, indicating that the photogenerated Fe^{2+} is involved in the photocatalytic CO_2 reduction. The ESR results suggest that the metal center (Fe) is the photocatalytically active site in the photocatalytic CO_2 reduction over MIL-101(Fe).

Since the metal center in MIL-101(Fe) is involved in the photocatlaytic CO_2 reduction, it is therefore interesting to investigate the photocatalytic performance of other Fe-containing MOF materials. MIL-53(Fe) and MIL-88B(Fe) were selected, since they both contain a BDC linker similar to that in MIL-101(Fe) but have different structures. The framework of MIL-53(Fe) contains chains of −OH corner-sharing FeO_6 octahedra, which are interconnected by BDC linkers to form one-dimensional pores.[18] MIL-88(Fe) is built up of oxo-centered Fe_3O trimers interconnected by linear BDC to form a 3D porous network that bears microporous channels and cages.[19] The formations of MIL-53(Fe) and MIL-88B(Fe) have also been confirmed by their XRD and TG data (Figures S12−S15, Supporting Information). Due to the existence of chains of −OH corner-sharing FeO_6 octahedra in MIL-53(Fe) and Fe_3O clusters in MIL-88B(Fe), both Fe-based MOFs also show absorption in the visible light region (Figures S16 and S17, Supporting Information).

The photocatalytic CO_2 reductions over MIL-53(Fe) and MIL-88B(Fe) were also carried out under visible light irradiation. The amount of $HCOO^-$ formed over MIL-53(Fe) reaches 29.7 μmol in 8 h, while that over MIL-88B(Fe) is only 9.0 μmol (Figures S18 and S19, Supporting Information). These values are much smaller than that observed over MIL-101(Fe) (59 μmol). The flat band positions for MIL-53(Fe) and MIL-88B(Fe) were also determined to be −0.70 and −0.48 V vs NHE (Figures S20 and S21). The band positions of the three Fe-based MOFs (MIL-101(Fe), MIL-53(Fe), and MIL-88B) do not correlate with their photocatalytic performance. Since all three MOF materials show comparable absorptions in the visible light region, it is proposed that factors other than the conduction band position and the light absorption ability should be responsible for their different photocatalytic performance in CO_2 reduction. MIL-53(Fe) and MIL-88B(Fe) are also quite stable during the photocatalytic CO_2 reduction, as evidenced from the XRD and TG data for the photocatalysts after the reaction (Figures S12−S15, Supporting Information).

As shown in Figure S22 (Supporting Information), the three investigated MOF materials exhibit quite different adsorption capabilities toward CO_2. At 1 atm and 273 K, MIL-101(Fe) shows the highest adsorption capability toward CO_2 (26.4 g/cm^3), while those over MIL-53(Fe) and MIL-88B(Fe) are only 13.5 and 10.4 g/cm^3, respectively. The in situ FT-IR technique has also been used to study the CO_2 adsorption process over these Fe-based MOF materials. As shown in Figure 5, the FT-IR spectrum of MIL-101(Fe) shows a new peak at 1253 cm^{-1} when CO_2 is introduced into the system, and its intensity increases with the amount of injected CO_2. Since the peak in this region (from 1250 to 1270 cm^{-1}) can be ascribed to the

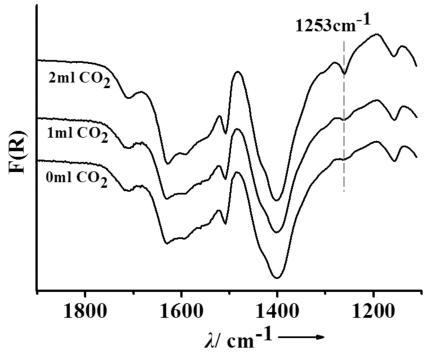

Figure 5. In situ FT-IR analyses of CO_2 adsorption over pretreated MIL-101(Fe).

dx.doi.org/10.1021/cs501169t | ACS Catal. 2014, 4, 4254−4260

bidentate carbonate coordinated to the metal center, the emergence of the peak at 1253 cm^{-1} over CO_2-saturated MIL-101(Fe) suggests the direct adsorption of CO_2 onto the Fe center.[20] The direct adsorption of CO_2 onto the Fe center is possible for MIL-101(Fe) since its structure contains coordination unsaturated Fe metal sites (CUSs).[21] Although the Fe center in MIL-101(Fe) is octahedrally coordinated, one of the terminal waters coordinated to the Fe center can be easily removed to give coordination unsaturated Fe metal sites (CUSs), which have been generally reported to act as the adsorption sites for molecular gases.[21,22] The in situ FT-IR of MIL-101(Fe) under a CO_2 atmosphere indicates that CO_2 is adsorbed directly onto the coordination unsaturated Fe sites in MIL-101(Fe). Although previously Metzler-Nolte et al. reported that CUSs can be generated on MIL-88B(Fe) under UHV at 500 K, the in situ FT-IR spectra do not show the direct adsorption of CO_2 over Fe sites in both MIL-53(Fe) and MIL-88B(Fe), suggesting that there exist no CUSs for CO_2 adsorption over these two MOFs under the current reaction conditions.[23] This is confirmed from the in situ FT-IR spectra of MIL-53(Fe) and MIL-88B(Fe) under a CO_2 atmosphere, which do not show any peaks in the region between 1250 and 1270 cm^{-1} (Figures S23 and S24, Supporting Information). As the ESR results suggest that the metal center (Fe) is the photocatalytically active site in the photocatalytic CO_2 reduction, the adsorption of CO_2 directly onto the metal center is advantageous for the photocatalytic CO_2 reduction reaction. Therefore, it is no wonder that MIL-101(Fe) with the coordination unsaturated sites (CUSs) shows the best photocatalytic performance for CO_2 reduction among these three Fe-based MOFs.

Previous studies revealed that although the Ti−O clusters in MIL-125(Ti) cannot be excited by visible light, the substitution of the linker BDC with 2-aminoterephthalic acid (ATA) can lead to visible-light-responsive NH_2-MIL-125(Ti) due to the antenna effect of the NH_2 functionality.[12a] To study the effect of a similar NH_2 functionality on the photocatalytic performance over these Fe-based MOF materials, amino-functionalized Fe-based MOF materials (NH_2-MIL-101(Fe), NH_2-MIL-53(Fe), and NH_2-MIL-88B(Fe)) have also been prepared and their photocatalytic performances for CO_2 reduction under visible light irradiation have been investigated.

NH_2-MIL-101(Fe), NH_2-MIL-53(Fe), and NH_2-MIL-88B(Fe) were prepared by following previously reported methods with slight modifications.[15a] The XRD patterns of the as-prepared amino-functionalized MOFs are similar to those of the parent MOFs (Figure 1; Figures S25 and S26, Supporting Information). However, the presence of the NH_2 functionality has been confirmed from the FT-IR spectra by peaks at around 3481 and 3377 cm^{-1}, which can be ascribed to the asymmetrical and symmetrical stretching vibrations of free primary amines without coordination (Figures S27−S29, Supporting Information).[24] Amino-functionalized MOFs with high quality have been obtained, as evidenced from the N_2 adsorption/desorption isotherms and TG analyses (Figures S30−S33, Supporting Information).

As expected, amino-functionalized Fe-based MOF materials show enhanced absorption in the visible light region (Figure 2; Figures S16 and S17, Supporting Information). The absorption edge of the as-prepared NH_2-MIL-101(Fe), NH_2-MIL-53(Fe) and NH_2-MIL-88B(Fe) extends to ca. 700 nm due to the existence of the NH_2 functionality. In addition to this, all of the amino-functionalized Fe-based MOF materials show improved adsorption capability toward CO_2 in comparison to those unfunctionalized MOFs (Figure S34, Supporting Information). At 1 atm and 273 K, the CO_2 uptakes are 34.0, 20.0, and 14.4 cm^3/g for NH_2-MIL-101(Fe), NH_2-MIL-53(Fe), and NH_2-MIL-88B(Fe) respectively, while those for the parent MIL-101(Fe), MIL-53(Fe), and MIL-88B(Fe) are only 26.4, 13.5, and 10.4 cm^3/g (Table 1). Such an enhancement in the adsorption capability toward CO_2 for amino-functionalized MOFs is within expectation, since both theoretical studies and experimental evidence have revealed that aromatic molecules functionalized with polar substituent groups can enhance the interactions between CO_2 and the functionalized aromatic molecules.[25]

Table 1. Comparisons of the CO_2 Adsorption and the Amount of $HCOO^-$ Produced over MIL-101(Fe), MIL-53(Fe), and MIL-88B(Fe) and Their Amino-Functionalized Derivatives

photocatalyst	amt of $HCOO^-$ produced (μmol)	CO_2 adsorption (cm^3/g)
NH_2-MIL-101(Fe)	178	34.0
MIL-101(Fe)	59.0	26.4
NH_2-MIL-53(Fe)	46.5	20.0
MIL-53(Fe)	29.7	13.5
NH_2-MIL-88(Fe)	30.0	14.4
MIL-88(Fe)	9.0	10.4

The photocatalytic reductions of CO_2 over amino-functionalized NH_2-MIL-101(Fe), NH_2-MIL-53(Fe), and NH_2-MIL-88B(Fe) have been investigated and compared with those of their parent MOFs (Table 1). It was found that all of the amino-functionalized MOFs show enhanced activity for photocatalytic CO_2 reduction. For NH_2-MIL-101(Fe), the amount of $HCOO^-$ formed reaches 178 μmol in 8 h, about 3.0-fold greater in comparison to that for the parent MIL-101(Fe) under otherwise similar conditions. Similarly, the amount of $HCOO^-$ formed over NH_2-MIL-53(Fe) and NH_2-MIL-88B(Fe) reaches 46.5 and 30.0 μmol in 8 h, while only 29.7 and 9 μmol of $HCOO^-$ are obtained for the parent MIL-53(Fe) and MIL-88B(Fe), respectively. The highest QE at 450 nm observed over NH_2-MIL-101(Fe) is determined to be 1.3×10^{-4}, which is comparable to that observed over a hybrid photocatalytic system containing a Ni complex (also an earth-abundant metal complex) coupled with a Ru photosensitizer (1.0×10^{-4}).[2h]

The wavelength dependence of the photocatalytic ability over MIL-101(Fe) and its amino-functionalized derivative has been studied to explore the mechanism for the enhancement of the photocatalytic performance over amino-functionalized Fe-based MOFs. The dependence of the amount of the produced $HCOO^-$ on the wavelength of incident light employed in NH_2-MIL-101(Fe) and MIL-101(Fe) is shown in Figure 6. The amount of the produced $HCOO^-$ over both NH_2-MIL-101(Fe) and MIL-101(Fe) is observed to depend strongly on the wavelength in a manner that correlates with their absorption intensities in the visible light region, indicating that the reactions over both photocatalysts are truly photocatalytic. When a 590 nm cutoff filter is used, no $HCOO^-$ is produced over MIL-101(Fe), while 5.6 μmol of $HCOO^-$ is still produced over NH_2-MIL-101(Fe). These findings indicate the following. (1) For nonmodified MIL-101(Fe), the Fe−O clusters can directly absorb visible light and transfer an electron from the

dx.doi.org/10.1021/cs501169t | ACS Catal. 2014, 4, 4254−4260

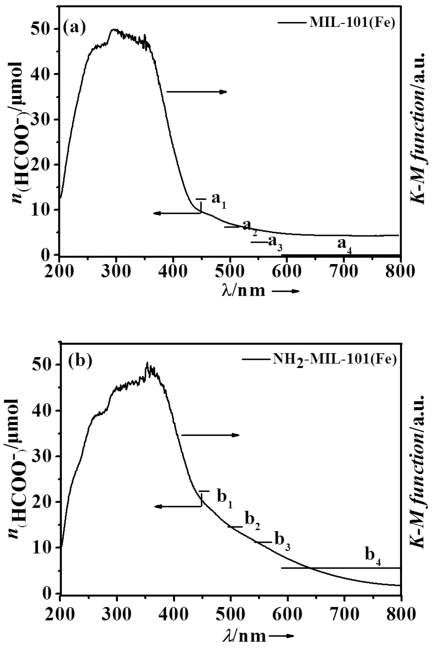

Figure 6. Dependence of the amount of produced $HCOO^-$ on the wavelength of incident light and the UV−vis DRS spectra of (a) MIL-101(Fe) and (b) NH_2-MIL-101(Fe). Wavelength region of irradiated light: (a_1, b_1) 440−455 nm; (a_2, b_2) 490−515 nm; (a_3, b_3) 537−566 nm; (a_4, b_4) above 590 nm. The wavelength region of irradiated light was controlled by using three different bandpass filters and a λ >590 nm cutoff filter.

O^{2-} to Fe^{3+} to form Fe^{2+}, which is capable to reduce CO_2. (2) For the amine-functionalized NH_2-MIL-101(Fe), in addition to the direct light absorption of the Fe−O cluster, the NH_2 functionality can also absorb light and transfer an electron from the organic linker to the Fe−O clusters to generate Fe^{2+} for CO_2 reduction in a manner expected for operation of an LCCT mechanism. (3) Although NH_2-MIL-101(Fe) also shows a 30% increase in its adsorption ability toward CO_2 in comparison to that of MIL-101(Fe), the almost 3-fold enhancement in its photocatalytic activity for CO_2 reduction in comparison to MIL-101(Fe) is much larger, indicating that the existence of the dual excitation pathways and the synergistic effect between these two pathways can promote the photocatalytic CO_2 reduction over amine-functionalized NH_2-MIL-101(Fe). A comparison of the QE for photocatalytic CO_2 reduction over those of NH_2-MIL-101(Fe) and MIL-101(Fe) at different wavelengths also indicates the existence of the dual excitation pathways (Table S1, Supporting Information).

On the basis of the above analysis, the mechanism for the enhancement of the photocatalytic CO_2 reduction over the amine-functionalized Fe-containing MOFs can be illustrated as shown in Scheme 1. As mentioned above, for nonmodified Fe-based MOF material, an excited charge separation state occurs by transferring an electron from the O^{2-} to Fe^{3+} in the Fe−O clusters upon visible light excitation. Fe^{3+} is thus reduced to Fe^{2+}, which is capable of reducing CO_2, whereas TEOA acts as an electron donor and hydrogen donor to achieve a complete photocatalytic cycle. Therefore, Fe-based MOF materials show photocatalytic activity for CO_2 reduction to give formate under visible light irradiation. For the amino-functionalized derivatives, in addition to the pathway of the direct excitation of the Fe−O clusters, there exists a second pathway via the excitation of the NH_2 functionality followed by an electron transfer from

Scheme 1. Dual Excitation Pathways over Amino-Functionalized Fe-Based MOFs

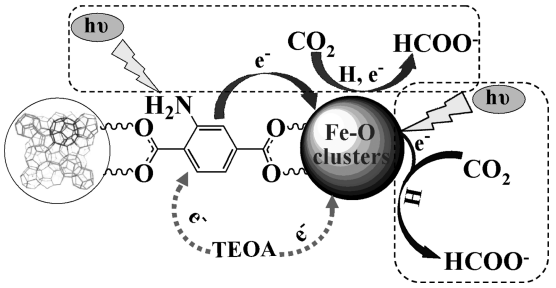

the excited organic linker to the metal center to generate Fe^{2+}. Such an excitation pathway is similar to that observed for the previously reported NH_2-MIL-125(Ti) and NH_2-Uio-66(Zr).[12] These two pathways can play synergetic roles in the excitation of these amino-functionalized Fe-based MOFs. In addition to this, the higher adsorption toward CO_2 induced by the NH_2 functionality for these amino-functionalized MOFs is also advantageous for the photocatalytic CO_2 reduction. The coexistence of dual excitation pathways on these amino-functionalized Fe-based MOFs and the enhanced adsorption capability toward CO_2 lead to their highly enhanced photocatalytic performance for CO_2 reduction. However, we observe a different enhanced degree of the photocatalytic performance for NH_2-MIL-101(Fe), NH_2-MIL-53(Fe), and NH_2-MIL-88B(Fe) in comparison to their nonfunctionalized counterparts (Table 1). At the current stage, we can only propose that the different enhancement degree may be related to the different efficiency of the electron transfer from the excited organic linker to the metal center in these three Fe-based MOF materials. More in-depth studies are still required to elucidate this.

CONCLUSIONS

In summary, Fe-based MOF materials (MIL-101(Fe), MIL-53(Fe), and MIL-88B(Fe)) show photocatalytic activity for CO_2 reduction under visible light irradiation in the presence of TEOA as a sacrificial agent. The direct excitation on the Fe−O clusters in these Fe-based MOF materials to induce electron transfer from O^{2-} to Fe^{3+} is responsible for their photocatalytic CO_2 reduction. Among these materials, MIL-101(Fe) shows the best activity for CO_2 reduction due to the existence of the coordination unsaturated Fe sites in its structure. An amine functionality on these Fe-based MOF materials can significantly enhance their photocatalytic activity for CO_2 reduction due to the synergetic effect of dual excitation pathways: i.e., an exciting NH_2 functionality followed by an electron transfer from the excited organic linker to the Fe center and the direct excitation of Fe−O clusters. This study gives us a better understanding of the photocatalytic CO_2 reduction over MOF-based materials and also provides some guidance for us in the development of visible-light-responsive photocatalysts for CO_2 reduction based on MOFs.

EXPERIMENTAL SECTION

Syntheses. All of the reagents were analytical grade and were used without further purifications. MIL-101(Fe), MIL-53(Fe), MIL-88B(Fe), and their NH_2-functionalzied derivatives were synthesized according to the literature. Briefly, MIL-101(Fe) and MIL-53(Fe) were prepared via a hydrothermal

dx.doi.org/10.1021/cs501169t | ACS Catal. 2014, 4, 4254−4260

treatment of $FeCl_3 \cdot 6H_2O$ and terephthalic acid (H_2BDC) (2:1) in DMF solvent at 110 and 170 °C, respectively, for 24 h. MIL-88B(Fe) was prepared hydrothermally from a 1/1 ratio of H_2BDC and $FeCl_3 \cdot 6H_2O$ in NaOH solution at 100 °C for 12 h. The NH_2-functionalized MIL-101(Fe) and MIL-88B(Fe) (NH_2-MIL-101(Fe) and NH_2-MIL-88B(Fe)) were prepared similarly to their parent MOFs except that H_2BDC was replaced by 2-aminoterephthalic acid (H_2ATA). NH_2-MIL-53(Fe) was prepared from a 1/1 molar ratio of ATA and $FeCl_3 \cdot 6H_2O$ in water at 150 °C for 72 h.

Characterizations. X-ray diffraction (XRD) patterns were collected on a Bruker D8 Advance X-ray diffractometer with Cu Kα radiation (λ = 0.15406 nm). IR spectra on KBr pellets of the samples were recorded on a Nicolet 410 FT-IR spectrometer at a resolution of 4 cm^{-1}. The in situ FTIR experiments were performed in an IR cell made of quartz. The cell comprises a pair of CaF_2 windows and is connected to a vacuum line. Before the FTIR measurements were initiated, the sample was treated under dynamic vacuum at 150 °C for 5 h. After the sample was cooled to room temperature, a different volume of CO_2 was injected into the cell with a syringe. After adsorption equilibrium was reached, an FTIR spectrum was collected. The Brunauer–Emmett–Teller (BET) surface area and CO_2 adsorption isotherm were measured with an ASAP2020 M instrument (Micromeritics Instrument Corp). The samples were degassed under vacuum at 150 °C for 10 h, the N_2 adsorption/desorption isotherms were measured at −196 °C, and CO_2 adsorption isotherms were measured at 0 °C. Thermogravimetric (TG) analyses were carried out on a PerkinElmer TGA7 instrument and measured from 50 to 700 °C at a heating rate of 5 °C/min in air. UV–vis diffuse reflectance spectra (UV–vis DRS) of the powder were obtained for the dry-pressed disk samples using a UV–vis spectrophotometer (Cary 500 Scan spectrophotometer, Varian). ^{13}C NMR analysis was measured in a CD_3CN/TEOA (5/1 v/v) solution using a Bruker AVANCE III 500 M system. The spectra were recorded under the following conditions: acquisition time 1.1 s; ca. 27600 times integration. Electron spin resonance (ESR) spectra were obtained with a Bruker ESP 300E electron paramagnetic resonance spectrometer at room temperature. The samples were placed in an ESR sample tube equipped with a stopcock valve, and the whole device was connected to a vacuum system. Prior to measurement, the ESR tube was vacuumed to remove the air.

Photocatalytic Reaction. A 50 mg portion of photocatalyst was evacuated and purged several times with CO_2. An MeCN and TEOA solution (60 mL, 5/1 v/v), predegassed with CO_2 to remove the dissolved O_2, was injected into the reaction flask. Then the solutions were irradiated with a 300 W Xe lamp with a UV-cut filter to remove light with wavelengths less than 420 nm and an IR-cut filter to remove all wavelengths longer than 800 nm. The products in the liquid phase were analyzed using an IC (881 Compact IC pro, Metrosep) with Metrosep A supp 5250/4.0 column. The gaseous reaction products were analyzed using a GC-TCD instrument (Shimadzu GC-2014) with a 5 Å molecular sieve packing column.

■ ASSOCIATED CONTENT

Supporting Information

The following files are available free of charge on the ACS Publications website at DOI: 10.1021/cs501169t.

Additional characterization data and photocatalytic results (PDF)

■ AUTHOR INFORMATION

Corresponding Author

*Z.L.: e-mail, zhaohuili1969@yahoo.com; tel (fax), 86-591-83779260.

Author Contributions

†These authors (D.W. and R.H.) contributed equally to this manuscript.

Notes

The authors declare no competing financial interest.

■ ACKNOWLEDGMENTS

This work was supported by the NSFC (21273035), 973 Programs (2014CB239303), and Specialized Research Fund for the Doctoral Program of Higher Education (20123514110002). Z.L. thanks the Award Program for Minjiang Scholar Professorship for financial support.

■ REFERENCES

(1) (a) Alessandro, D. M. D.; Smit, B.; Long, J. R. *Angew. Chem., Int. Ed.* **2010**, *49*, 6058–6082. (b) DuBois, M. R.; DuBois, D. L. *Acc. Chem. Res.* **2009**, *42*, 1974–1982. (c) Cokoja, M.; Bruckmeier, C.; Rieger, B.; Herrmann, W. A.; Kühn, F. E. *Angew. Chem., Int. Ed.* **2011**, *50*, 8510–8538.

(2) (a) Inoue, T.; Fujishima, A.; Konishi, S.; Honda, K. *Nature* **1979**, *277*, 637–638. (b) Tong, H.; Ouyang, S. X.; Bi, Y. P.; Umezawa, N.; Oshikiri, M.; Ye, J. H. *Adv. Mater.* **2012**, *24*, 229–251. (c) Matsuoka, M.; Anpo, M. *J. Photochem. Photobiol. C* **2003**, *3*, 225–252. (d) Lin, W.; Frei, H. *J. Am. Chem. Soc.* **2005**, *127*, 1610–1611. (e) Habisreutinger, S. N.; Schmidt-Mende, L.; Stolarczyk, J. K. *Angew. Chem., Int. Ed.* **2013**, *52*, 7372–7408. (f) Tamaki, Y.; Morimoto, T.; Koike, K.; Ishitani, O. *Proc. Natl. Acad. Sci. U.S.A.* **2012**, *109*, 15673–15678. (g) Sato, S.; Morikawa, T.; Kajino, T.; Ishitani, O. *Angew. Chem., Int. Ed.* **2013**, *52*, 988–992. (h) Sara Thoi, V.; Kornienko, N.; Margarit, C. G.; Yang, P.; Chang, C. J. *J. Am. Chem. Soc.* **2013**, *135*, 14413–14424.

(3) (a) Meek, S. T.; Greathouse, J. A.; Allendorf, M. D. *Adv. Mater.* **2011**, *23*, 249–267. (b) Férey, G.; Serre, C.; Devic, T.; Maurin, G.; Jobic, H.; Llewellyn, P. L.; De Weireld, G.; Vimont, A.; Daturi, M.; Chang, J.-S. *Chem. Soc. Rev.* **2011**, *40*, 550–562. (c) Gascon, J.; Corma, A.; Kapteijn, F.; Llabres i Xamena, F. X. *ACS Catal.* **2014**, *4*, 361–378. (d) Abedi, S.; Morsali, A. *ACS Catal.* **2014**, *4*, 1398–1403.

(4) Li, J.-R.; Kuppler, R. J.; Zhou, H.-C. *Chem. Soc. Rev.* **2009**, *38*, 1477–1504.

(5) Chen, B.; Xiang, S.; Qian, G. *Acc. Chem. Res.* **2010**, *43*, 1115–1124.

(6) Qiu, S.; Zhu, G. *Coord. Chem. Rev.* **2009**, *253*, 2891–2911.

(7) Czaja, A. U.; Trukhan, N.; Müller, U. *Chem. Soc. Rev.* **2009**, *38*, 1284–1293.

(8) (a) Keskin, S.; Kızılel, S. *Ind. Eng. Chem. Res.* **2011**, *50*, 1799–1812. (b) McKinlay, A. C.; Morris, R. E.; Horcajada, P.; Férey, G.; Gref, R.; Couvreur, P.; Serre, C. *Angew. Chem., Int. Ed.* **2010**, *49*, 6260–6266. (c) Dhakshinamoorthy, A.; Alvaro, M.; Garcia, H. *ACS Catal.* **2011**, *1*, 836–840. (d) Khajavi, H.; Stil, H. A.; Kuipers, H. P. C. E.; Gascon, J.; Kapteijn, F. *ACS Catal.* **2013**, *3*, 2617–2626.

(9) (a) Corma, A.; Garcia, H.; Llabrés i Xamena, F. X. *Chem. Rev.* **2010**, *110*, 4606–4655. (b) Lee, J.; Farha, O. K.; Roberts, J.; Scheidt, K. A.; Nguyen, S. T.; Hupp, J. T. *Chem. Soc. Rev.* **2009**, *38*, 1450–1459. (c) Farrusseng, D.; Aguado, S.; Pinel, C. *Angew. Chem., Int. Ed.* **2009**, *48*, 7502–7513. (d) Ma, L. Q.; Abney, C.; Lin, W. B. *Chem. Soc. Rev.* **2009**, *38*, 1248–1256. (e) Gu, X. J.; Lu, Z. H.; Jiang, H. L.; Akita, T.; Xu, Q. *J. Am. Chem. Soc.* **2011**, *133*, 11822–11825. (f) Yuan, B. Z.; Pan, Y. Y.; Li, Y. W.; Yin, B. L.; Jiang, H. F. *Angew. Chem., Int. Ed.* **2010**, *49*, 4054–4058. (g) Xuan, W.; Zhu, C. F.; Liu, Y.; Cui, Y. *Chem.*

Soc. Rev. **2012**, *41*, 1677−1695. (h) Lykourinou, V.; Chen, Y.; Wang, X. S.; Meng, L.; Hoang, T.; Ming, L.; Musselman, R. L.; Ma, S. Q. *J. Am. Chem. Soc.* **2011**, *133*, 10382−10385.
(10) (a) Llabrés i Xamena, F. X.; Corma, A.; Garcia, H. *J. Phys. Chem. C* **2007**, *111*, 80−85 DOI: 10.1021/jp063600e. (b) Tachikawa, T.; Choi, J. R.; Fujitsuka, M.; Majima, T. *J. Phys. Chem. C* **2008**, *112*, 14090−14101.
(11) (a) Wang, J. L.; Wang, C.; Lin, W. B. *ACS Catal.* **2012**, *2*, 2630−2640. (b) Alvaro, M.; Carbonell, E.; Ferrer, B.; Llabrés i Xamena, F. X.; Garcia, H. *Chem. Eur. J.* **2007**, *13*, 5106−5112. (c) Gascon, J.; Hernandez-Alonso, M. D.; Almeida, A. R.; Klink, G. P. M.; Kapteijn, F.; Mul, G. *ChemSusChem* **2008**, *1*, 981−983. (d) Kataoka, Y.; Sato, K.; Miyazaki, Y.; Masuda, K.; Tanaka, H.; Naito, S.; Mori, W. *Energy Environ. Sci.* **2009**, *2*, 397−400. (e) Das, M. C.; Xu, H.; Wang, Z.; Srinivas, G.; Zhou, W.; Yue, Y.; Nesterov, V. N.; Qian, G.; Chen, B. *Chem. Commun.* **2011**, *47*, 11715−11717. (f) Wang, C.; Xie, Z.; deKrafft, K. E.; Lin, W. B. *J. Am. Chem. Soc.* **2011**, *133*, 13445−13454. (g) Laurier, K. G. M.; Vermoortele, F.; Ameloot, R.; De Vos, D. E.; Hofkens, J.; Roeffaers, M. B. J. *J. Am. Chem. Soc.* **2013**, *135*, 14488−14491. (h) Modrow, A.; Zargarani, D.; Herges, R.; Stock, N. *Dalton Trans.* **2012**, *41*, 8690−8696. (i) Wang, C.; Lin, W. B. *J. Am. Chem. Soc.* **2011**, *133*, 4232−4235. (j) Song, F. F.; Wang, C.; Falkowski, J. M.; Ma, Q.; Lin, W. *J. Am. Chem. Soc.* **2010**, *132*, 15390−15398. (k) Sato, S.; Morikawa, T.; Saeki, S.; Kajino, T.; Motohiro, T. *Angew. Chem., Int. Ed.* **2010**, *49*, 5101−5105.
(12) (a) Fu, Y. H.; Sun, D. R.; Chen, Y. J.; Huang, R. K.; Ding, Z. X.; Fu, X. Z.; Li, Z. H. *Angew. Chem., Int. Ed.* **2012**, *51*, 3364−3367. (b) Sun, D. R.; Fu, Y. H.; Liu, W. J.; Ye, L.; Wang, D. K.; Yang, L.; Fu, X. Z.; Li, Z. H. *Chem. Eur. J.* **2013**, *19*, 14279−14285.
(13) (a) Sun, W. T.; Meng, Q. Q.; Jing, L. Q.; Liu, D. N.; Cao, Y. *J. Phys. Chem. C* **2013**, *117*, 1358−1365. (b) Hattori, H.; Ide, Y.; Ogo, S.; Inumaru, K.; Sadakane, M.; Sano, T. *ACS Catal.* **2012**, *2*, 1910−1915. (c) Ziebart, C.; Federsel, C.; Anbarasan, P.; Jackstell, R.; Baumann, W.; Spannenberg, A.; Beller, M. *J. Am. Chem. Soc.* **2012**, *134*, 20701−20704.
(14) (a) Li, Y.; Feng, Z. C.; Xin, H. C.; Fan, F. T.; Zhang, J.; Magusin, P. C. M. M.; Hensen, E. J. M.; van Santen, R. A.; Yang, Q. H.; Li, C. *J. Phys. Chem. B* **2006**, *110*, 26114−26121. (b) Bordiga, S.; Buzzoni, R.; Geobaldo, F.; Lamberti, C.; Giamello, E.; Zecchina, A.; Leofanti, G.; Petrini, G.; Tozzola, G.; Vlaic, G. *J. Catal.* **1996**, *158*, 486−501.
(15) (a) Bauer, S.; Serre, C.; Devic, T.; Horcajada, P.; Marrot, J.; Férey, G.; Stock, N. *Inorg. Chem.* **2008**, *47*, 7568−7576. (b) Lupu, D.; Ardelean, O.; Blanita, G.; Borodi, G.; Lazar, M. D.; Biris, A. R.; Ioan, C.; Mihet, M.; Misan, I.; Popeneciu, G. *Int. J. Hydrogen Energy* **2011**, *36*, 3586−3592.
(16) Matsumoto, Y.; Omae, K.; Watanabe, I.; Sato, E. *J. Electrochem. Soc.* **1986**, *133*, 711−716.
(17) (a) Nishikawa, M.; Mitani, Y.; Nosaka, Y. *J. Phys. Chem. C* **2012**, *116*, 14900−14907. (b) Vinu, A.; Krithiga, T.; Balasubramanian, V. V.; Asthana, A.; Srinivasu, P.; Mori, T.; Ariga, K.; Ramanath, G.; Ganesan, P. G. *J. Phys. Chem. B* **2006**, *110*, 11924−11931.
(18) (a) Llewellyn, P. L.; Horcajada, P.; Maurin, G.; Devic, T.; Rosenbach, N.; Bourrelly, S.; Serre, C.; Vincent, D.; Loera-Serna, S.; Filinchuk, Y.; Férey, G. *J. Am. Chem. Soc.* **2009**, *131*, 13002−13008. (b) Haque, E.; Khan, N. A.; Park, J. H.; Jhung, S. H. *Chem.?Eur. J.* **2010**, *16*, 1046−1052.
(19) (a) Ma, M. Y.; Bétard, A.; Weber, I.; Al-Hokbany, N. S.; Fischer, R. A.; Metzler-Nolte, N. *Cryst. Growth Des.* **2013**, *13*, 2286−2291. (b) Dhakshinamoorthy, A.; Alvaro, M.; Chevreau, H.; Horcajada, P.; Devic, T.; Serre, C.; Garcia, H. *Catal. Sci. Technol.* **2012**, *2*, 324−330.
(20) Stevens, R. W., Jr.; Siriwardane, R. V.; Logan, J. *Energy Fuels* **2008**, *22*, 3070−3079.
(21) (a) Chowdhury, P.; Bikkina, C.; Gumma, S. *J. Phys. Chem. C* **2009**, *113*, 6616−6621. (b) Hwang, Y. K.; Hong, D. Y.; Chang, J. S.; Jhung, S. H.; Seo, Y. K.; Kim, J.; Vimont, A.; Daturi, M.; Serre, C.; Férey, G. *Angew. Chem., Int. Ed.* **2008**, *47*, 4144−4148.
(22) (a) Chen, L. J.; Morrison, C. A.; Duren, T. *J. Phys. Chem. C* **2012**, *116*, 18899−18909. (b) Valvekens, P.; Vermoortele, F.; De Vos, D. *Catal. Sci. Technol.* **2013**, *3*, 1435−1445. (c) Hou, X. J.; He, P.; Li, H. Q.; Wang, X. R. *J. Phys. Chem. C* **2013**, *117*, 2824−2834.
(23) Ma, M.; Noei, H.; Mienert, B.; Niesel, J.; Bill, E.; Muhler, M.; Fischer, R. A.; Wang, Y. M.; Schatzschneider, U.; Metzler-Nolte, N. *Chem. Eur. J.* **2013**, *19*, 6785−6790.
(24) Serra-Crespo, P.; Ramos-Fernandez, E. V.; Gascon, J.; Kapteijn, F. *Chem. Mater.* **2011**, *23*, 2565−2572.
(25) (a) Arstad, B.; Fjellvag, H.; Kongshaug, K. O.; Swang, O.; Blom, R. *Adsorption* **2008**, *14*, 755−762. (b) Demessence, A.; D'Alessandro, D. M.; Foo, M. L.; Long, J. R. *J. Am. Chem. Soc.* **2009**, *131*, 8784−8786. (c) Chen, Z. X.; Xiang, S. C.; Arman, H. D.; Li, P.; Steven, T.; Zhao, D. Y.; Chen, B. L. *Eur. J. Inorg. Chem.* **2011**, 2227−2231 DOI: 10.1002/ejic.201100034.